Angewandte Chemie
Eine Zeitschrift der Gesellschaft Deutscher Chemiker

Supporting Information

69451 Weinheim, Germany

Mechanistic Role of Water on the Rate and Selectivity of Fischer–Tropsch Synthesis on Ruthenium Catalysts**

David D. Hibbitts, Brett T. Loveless, Matthew Neurock, and Enrique Iglesia**

anie_201304610_sm_miscellaneous_information.pdf

Supporting Information

Table of Contents

*I. Reaction Coordinate Diagrams Comparing Routes via COH**

An alternative mechanism for H-assisted CO* activation occurring via COH* is the quasi-equilibrated formation of COH* followed by a simultaneous O-H bond formation and C-O bond activation to form C* and H_2O, referred to here as the "carbon adatom route". During anhydrous CO activation or H_2O-mediated CO activation, this route was found to be less favorable than the hydroxymethylidyne route described in the main text.

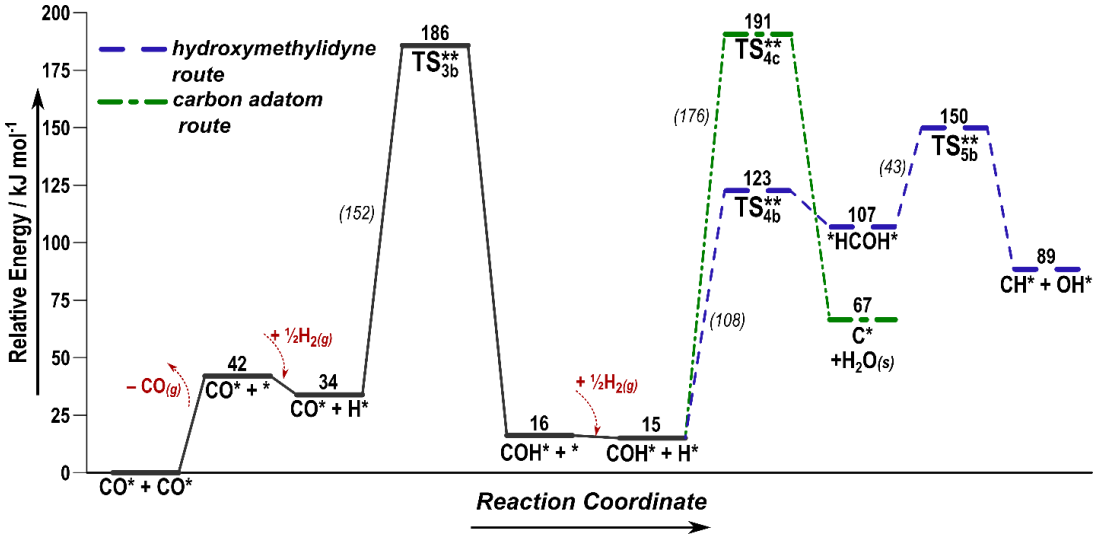

Figure S1. DFT-calculated reaction coordinate diagrams for H*-assisted CO activation mechanisms via COH* (hydroxymethylidyne and carbon routes). As shown, the two routes share the COH* + H* intermediate. The carbon adatom route has an effective barrier of 191 kJ mol^{-1} compared to an effective barrier of 150 kJ mol^{-1} for the hydroxymethylidyne route.

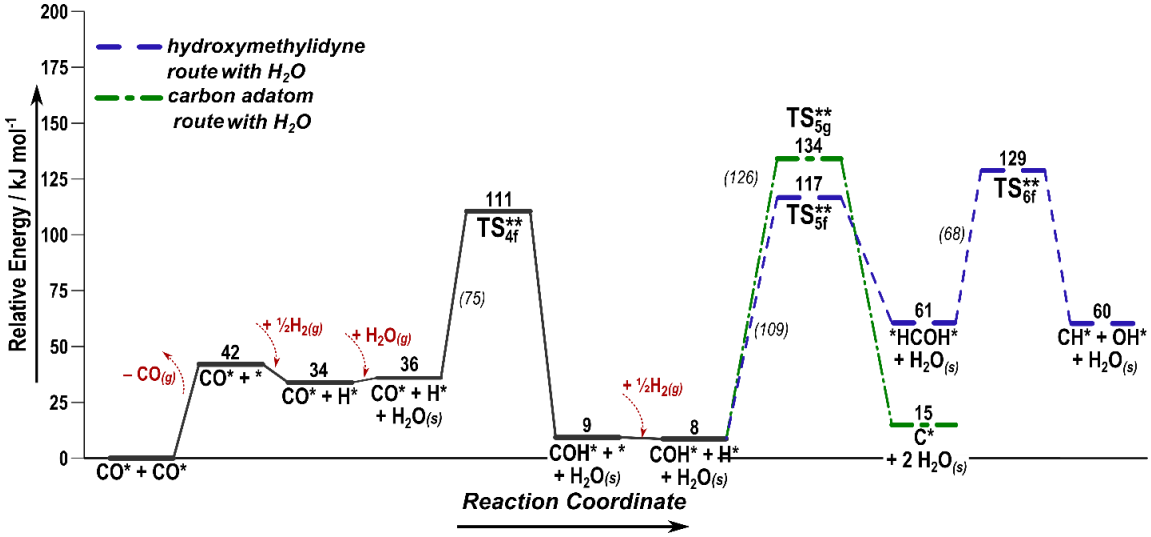

Figure S2. DFT-calculated reaction coordinate diagrams for H-assisted CO activation mechanisms via COH* (hydroxymethylidyne and carbon adatom routes) in the presence of H_2O. As shown, the two routes share the COH* + H* + $H_2O(s)$ intermediate. The carbon adatom route has an effective barrier of 134 kJ mol^{-1} compared to an effective barrier of 129 kJ mol^{-1} for the hydroxymethylidyne route.

II. Reaction Energies, Barriers and Effective Barriers for H-Assisted CO Activation Routes

DFT calculated reaction energies, intrinsic and effective activation energies for all of the elementary steps involved in the anhydrous as well as the H_2O-mediated H-assisted CO activation paths are given in Tables S1 and S2, respectively. The equations for the effective activation energies for each step are defined and used to along with the DFT energies to determine the effective activation energies for each of the elementary steps.

Table S1. Reaction energies and equations for effective barriers for anhydrous H-assisted CO activation routes.

Step	*Reaction*	ΔE_{rxn} *kJ mol^{-1}*	ΔE_{act} *kJ mol^{-1}*	ΔE_{eff} *kJ mol^{-1}*	*Eq. for* ΔE_{eff}
1	CO* + CO* ⇌ CO* + * + CO*(g)*	42			
2	H_2*(g)* + 2* ⇌ 2H*	-8			
3a	CO* + H* ⇌ HCO* + *	63	93	127	$\Delta E_{eff} = E_{TS_i^{**}} + E_{CO(g)} - 2E_{CO*} - {}^{n}/_{2}\, E_{H_2(g)}$
4a	HCO* + H* ⟶ *HCOH*	9	96	193	$\Delta E_{eff} = E_{TS_{4a}^{**}} + E_{CO(g)} - 2E_{CO*} - E_{H_2(g)}$
5a	*HCOH* ⟶ CH* + OH*	-18	43	150	$\Delta E_{eff} = E_{TS_{5a}^{**}} + E_{CO(g)} - 2E_{CO*} - E_{H_2(g)}$
3b	CO* + H* ⇌ COH* + *	-18	152	186	$\Delta E_{eff} = E_{TS_{3b}^{**}} + E_{CO(g)} - 2E_{CO*} - ½\, E_{H_2(g)}$
4b	COH* + H* ⟶ *HCOH*	92	108	123	$\Delta E_{eff} = E_{TS_{4b}^{**}} + E_{CO(g)} - 2E_{CO*} - E_{H_2(g)}$
5b	*HCOH* ⟶ CH* + OH*	-18	43	150	$\Delta E_{eff} = E_{TS_{5b}^{**}} + E_{CO(g)} - 2E_{CO*} - E_{H_2(g)}$
3c	CO* + H* ⇌ COH* + *	-18	152	186	$\Delta E_{eff} = E_{TS_{3c}^{**}} + E_{CO(g)} - 2E_{CO*} - ½\, E_{H_2(g)}$
4c	COH* + H* ⟶ C* + * + H_2O*(s)*	52	176	191	$\Delta E_{eff} = E_{TS_{4c}^{**}} + E_{CO(g)} - 2E_{CO*} - E_{H_2(g)}$

Table S2. Reaction energies and equations for effective barriers for H_2O-mediated H-assisted CO activation routes.

Step	*Reaction*	ΔE_{rxn} *kJ mol^{-1}*	ΔE_{act} *kJ mol^{-1}*	ΔE_{eff} *kJ mol^{-1}*	*Eq. for* ΔE_{eff}
1	CO* + CO* ⇌ CO* + * + CO*(g)*	42			
2	H_2*(g)* + 2* ⇌ 2H*	-8			
3e/f/g	CO* + H_2O*(g)* ⇌ CO*···H_2O*(s)*	2			
4e	CO*···H_2O*(s)* + H* ⇌ HCO*···H_2O*(s)* + *	63	93	127	$\Delta E_{eff} = E_{TS_i^{**}} + E_{CO(g)} - 2E_{CO*} - {}^{n}/_{2}\, E_{H_2(g)} - E_{H_2O(g)}$
5e	HCO*···H_2O*(s)* + H* ⟶ *HCOH*···H_2O*(s)*	-38	82	181	$\Delta E_{eff} = E_{TS_{5e}^{**}} + E_{CO(g)} - 2E_{CO*} - E_{H_2(g)} - E_{H_2O(g)}$
6e	*HCOH*···H_2O*(s)* ⟶ CH* + OH*···H_2O*(s)*	0	69	129	$\Delta E_{eff} = E_{TS_{6e}^{**}} + E_{CO(g)} - 2E_{CO*} - E_{H_2(g)} - E_{H_2O(g)}$
4f	CO*···H_2O*(s)* + H* ⇌ COH*···H_2O*(s)* + *	-47	75	111	$\Delta E_{eff} = E_{TS_{4f}^{**}} + E_{CO(g)} - 2E_{CO*} - ½\, E_{H_2(g)} - E_{H_2O(g)}$
5f	COH*···H_2O*(s)* + H* ⟶ *HCOH*···H_2O*(s)*	72	108	117	$\Delta E_{eff} = E_{TS_{5f}^{**}} + E_{CO(g)} - 2E_{CO*} - E_{H_2(g)} - E_{H_2O(g)}$
6f	*HCOH*···H_2O*(s)* ⟶ CH* + OH*···H_2O*(s)*	0	69	129	$\Delta E_{eff} = E_{TS_{6f}^{**}} + E_{CO(g)} - 2E_{CO*} - E_{H_2(g)} - E_{H_2O(g)}$
4g	CO*···H_2O*(s)* + H* ⇌ COH*···H_2O*(s)* + *	-47	75	111	$\Delta E_{eff} = E_{TS_{4g}^{**}} + E_{CO(g)} - 2E_{CO*} - ½\, E_{H_2(g)} - E_{H_2O(g)}$
5g	COH*···H_2O*(s)* + H* ⟶ C*···$2H_2O$*(s)* + *	26	125	134	$\Delta E_{eff} = E_{TS_{5g}^{**}} + E_{CO(g)} - 2E_{CO*} - E_{H_2(g)} - E_{H_2O(g)}$

III. Derivation of Rate Expressions and Effective Barriers

1) Formyl Route, Anhydrous Case at Low H_2O Pressure

DFT-derived reaction coordinate diagram:

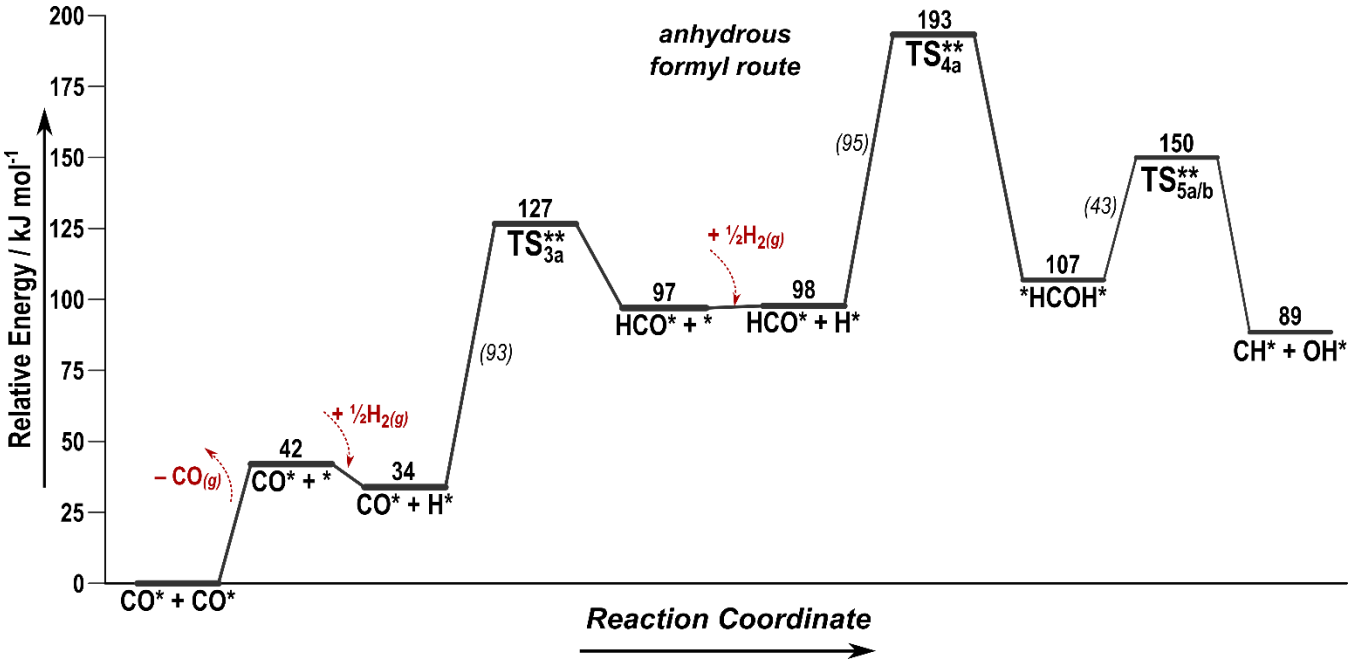

Figure S3. Reaction coordinate diagram for the H-assisted activation of CO via the anhydrous formyl route.

- Based on DFT-derived energies, the formation of HCO* is considered quasi-equilibrated as its reverse activation barrier (30 kJ mol^{-1}) is lower than the forward barrier to form *HCOH* (96 kJ mol^{-1}).
- The formation of *HCOH* is irreversible as its reverse barrier (86 kJ mol^{-1}) is higher than the forward barrier to form CH* and OH* (43 kJ mol^{-1}).
- For this mechanism, the formation of *HCOH* is considered the kinetically-relevant step.

Mechanism:

1) $CO_{(g)} + * \rightleftharpoons CO^*$ $\quad [CO^*] = K_{CO}(CO)[*]$

2) $H_{2(g)} + 2* \rightleftharpoons 2H^*$ $\quad [H^*] = K_{H_2}^{0.5}(H_2)^{0.5}[*]$

3a) $H^* + CO^* \rightleftharpoons HCO^* + *$ $\quad [HCO^*] = K_{3a}[CO^*][H^*][*]^{-1} = K_{3a}K_{CO}K_{H_2}^{0.5}(CO)(H_2)^{0.5}[*]$

4a) $H^* + HCO^* \longrightarrow {}^*HCOH^*$ $\quad r_{4a} = k_{4a}[H^*][HCO^*]L^{-1} = k_{4a}K_{3a}K_{CO}K_{H_2}(CO)(H_2)[*]^2L^{-1}$

5a) $^*HCOH^* \longrightarrow CH^* + OH^*$

Site Balance:

This rate expression is only valid at low H_2O pressures, under such conditions no H_2O-derived intermediates are expected to block surface sites.

$$L = [*] + [CO^*]$$

$$\frac{L}{[*]} = 1 + \frac{[CO^*]}{[*]} = 1 + K_{CO}(CO)$$

$$\frac{[*]^2}{L^2} = \frac{1}{[1 + K_{CO}(CO)]^2}$$

Rate Expression:

$$r_{CO} = \frac{r_{4a}}{L} = \frac{k_{4a}K_{3a}K_{CO}K_{H_2}(CO)(H_2)}{[1+K_{CO}(CO)]^2} \quad (1)$$

at high CO pressure:

$$r_{CO} = \frac{k_{4a}K_{3a}K_{H_2}(H_2)}{K_{CO}(CO)} \quad (2)$$

Effective energy barrier at high CO pressure:

$$\Delta E_{eff} = -Q_{CO} + Q_{H_2} + \Delta E_{Rxn,3a} + \Delta E_{Act,4a} \quad (3)$$

$$= \left(E_{CO(g)} + E_* - E_{CO^*}\right) + \left(2E_{H^*} - 2E_* - E_{H_2(g)}\right) + \left(E_{HCO^*} + E_* - E_{H^*} - E_{CO^*}\right) + \left(E_{TS_{4a}^{**}} - E_{HCO^*} - E_{H^*}\right) \quad (4)$$

$$= E_{TS_{4a}^{**}} + E_{CO(g)} - 2E_{CO*} - E_{H_2(g)} \quad (5)$$

$$= \mathbf{193}\ kJ\ mol^{-1}$$

2) Hydroxymethylidyne route, anhydrous case at low H_2O pressure

DFT-derived reaction coordinate diagram:

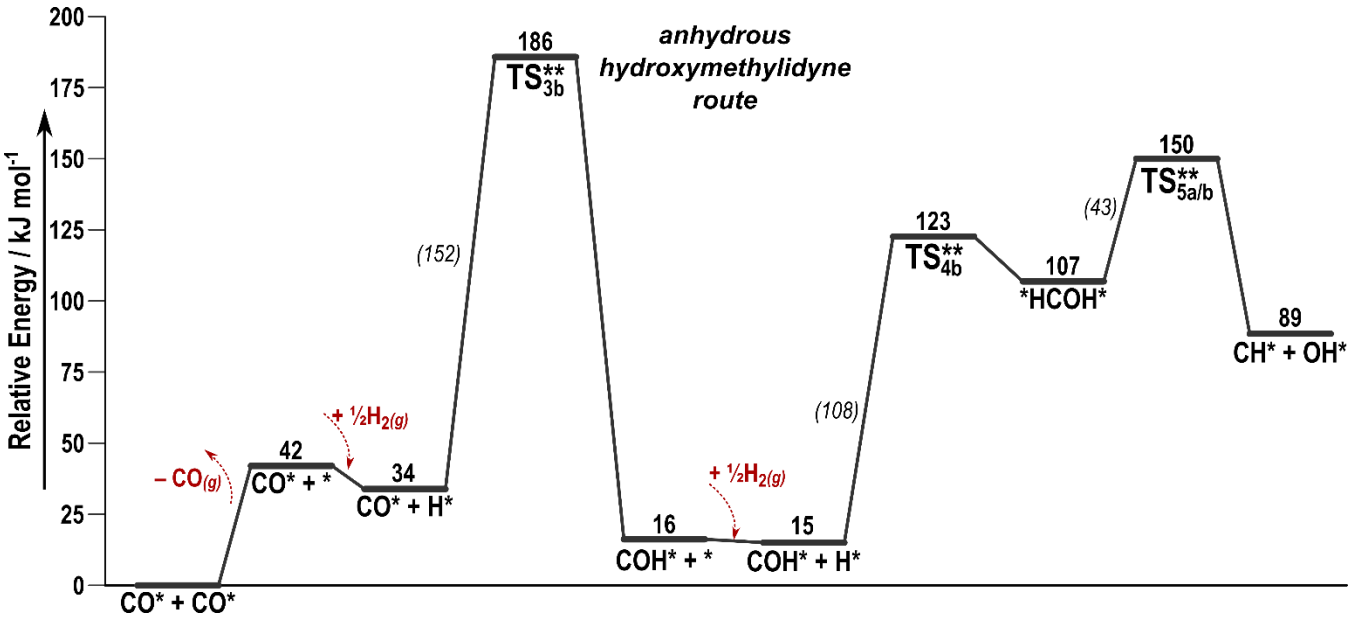

Figure S4. Reaction coordinate diagram for the H-assisted activation of CO via the anhydrous hydroxymethylidyne route.

- Based on the DFT-derived reaction energies, the formation of COH* is considered irreversible as its reverse activation barrier (170 kJ mol^{-1}) is higher than the forward barrier to form *HCOH* (107 kJ mol^{-1}) or dissociate *HCOH* (134 kJ mol^{-1}).
- For this mechanism, the formation of COH* is considered the kinetically-relevant step.

Mechanism:

1) $CO_{(g)} + * \rightleftharpoons CO^*$ $\quad [CO^*] = K_{CO}(CO)[*]$

2) $H_{2(g)} + 2* \rightleftharpoons 2H^*$ $\quad [H^*] = K_{H_2}^{0.5}(H_2)^{0.5}[*]$

3b) $H^* + CO^* \longrightarrow HCO^* + *$ $\quad r_{3b} = k_{3b}[CO^*][H^*]L^{-1} = k_{3b}K_{CO}K_{H_2}^{0.5}(CO)(H_2)^{0.5}[*]$

4b) $H^* + HCO^* \longrightarrow {}^*HCOH^*$

5b) $^*HCOH^* \longrightarrow CH^* + OH^*$

Site Balance:

This rate expression is only valid at low H_2O pressures, under such conditions no H_2O-derived intermediates are expected to block surface sites.

$$L = [*] + [CO^*]$$

$$\frac{L}{[*]} = 1 + \frac{[CO^*]}{[*]} = 1 + K_{CO}(CO)$$

$$\frac{[*]^2}{L^2} = \frac{1}{[1 + K_{CO}(CO)]^2}$$

Rate Expression:

$$r_{CO} = \frac{r_{3b}}{L} = \frac{k_{3b} K_{CO} K_{H_2}^{0.5} (CO)(H_2)^{0.5}}{[1+K_{CO}(CO)]^2} \quad (6)$$

at high CO pressure:

$$r_{CO} = \frac{k_{3b} K_{H_2}^{0.5} (H_2)^{0.5}}{K_{CO}(CO)} \quad (7)$$

Effective energy barrier at high CO pressure:

$$\Delta E_{eff} = -Q_{CO} + ½\, Q_{H_2} + \Delta E_{Act,3b} \quad (8)$$

$$= \left(E_{CO(g)} + E_* - E_{CO^*}\right) + \left(E_{H^*} - E_* - ½\, E_{H_2(g)}\right) + \left(E_{TS_{3b}^{**}} - E_{CO^*} - E_{H^*}\right) \quad (9)$$

$$= E_{TS_{3b}^{**}} + E_{CO(g)} - 2E_{CO*} - ½\, E_{H_2(g)} \quad (10)$$

$$= \mathbf{186}\ kJ\ mol^{-1}$$

3) Formyl Route with water as a H-source for *HCOH* formation

DFT-derived reaction coordinate diagram:

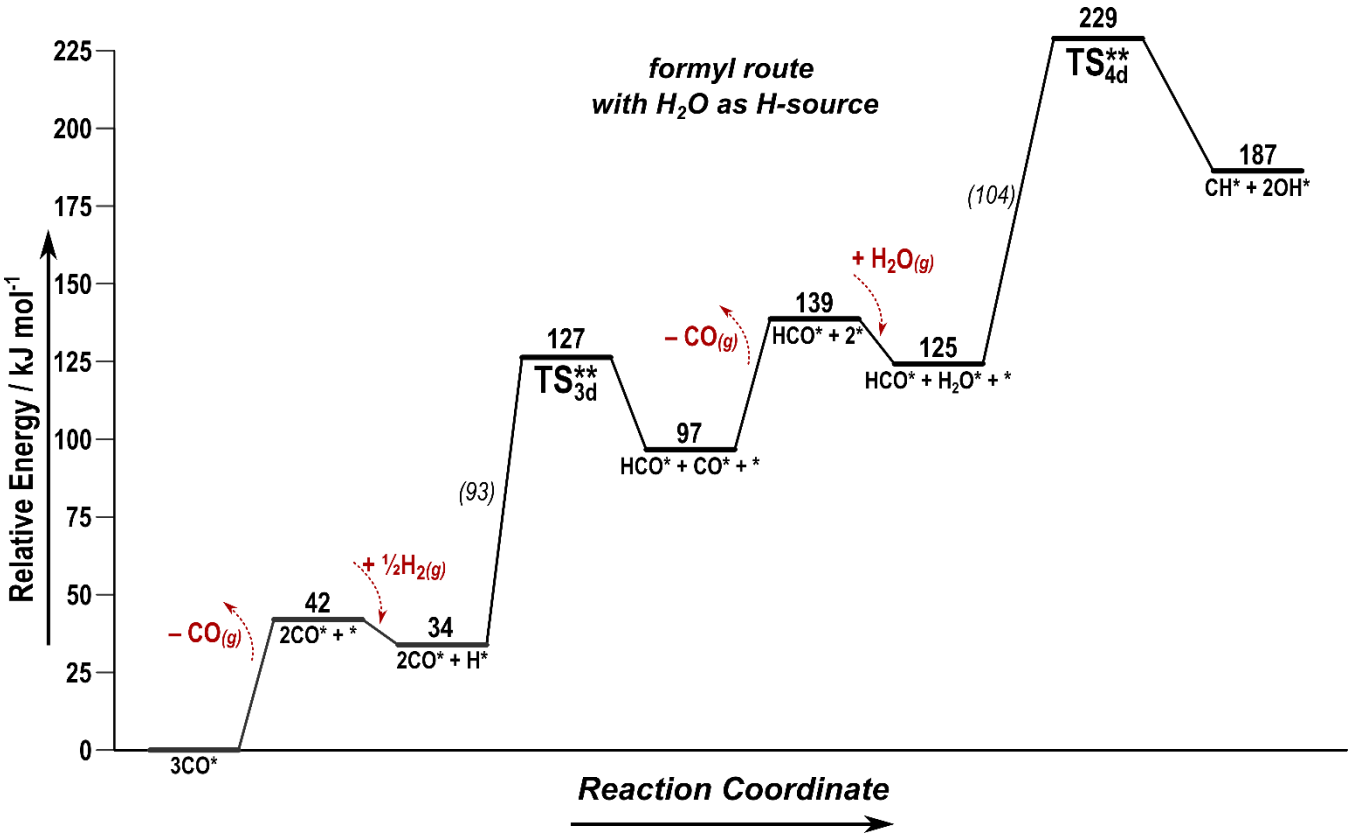

Figure S5. Reaction coordinate diagram for the formyl route with H_2O as a H-source in the formation of *HCOH*.

- Based on the DFT-derived reaction energies, the formation of HCO* is considered quasi-equilibrated as its reverse activation barrier (30 kJ mol^{-1}) is lower than the forward barrier to form *HCOH* (132 kJ mol^{-1}).
- For this mechanism, the formation of HCOH* is considered the kinetically-relevant step.

Mechanism

1)	$CO_{(g)} + * \rightleftharpoons CO^*$	$[CO^*] = K_{CO}(CO)[*]$
2)	$H_{2(g)} + 2* \rightleftharpoons 2H^*$	$[H^*] = K_{H_2}^{0.5}(H_2)^{0.5}[*]$
3d)	$H^* + CO^* \rightleftharpoons HCO^* + *$	$[HCO^*] = K_{3d}K_{CO}K_{H_2}^{0.5}(CO)(H_2)^{0.5}[*]$
4d)	$H_2O_{(g)} + * \rightleftharpoons H_2O^*$	$[H_2O^*] = K_{H_2O}(H_2O)[*]$
5d)	$HCO^* + H_2O^* + * \longrightarrow CH^* + 2OH^*$	$r_{5d} = k_{5d}[H_2O^*][HCO^*][*]L^{-2}$
		$= k_{5d}K_{3d}K_{CO}K_{H_2}^{0.5}K_{H_2O}(CO)(H_2)^{0.5}(H_2O)[*]^3L^{-2}$

Formation of Site Blocking Intermediates:

$H_2O^* + * \rightleftharpoons OH^* + H^*$ $\quad [OH^*] = K_{OH}(H_2O)(H_2)^{-0.5}[*]$

$OH^* + * \rightleftharpoons O^* + H^*$ $\quad [O^*] = K_O(H_2O)(H_2)^{-1}[*]$

Site Balance:

$$L = [*] + [CO^*] + [H_2O^*] + [OH^*] + [O^*]$$

$$\frac{L}{[*]} = 1 + \frac{[CO^*]}{[*]} + \frac{[H_2O^*]}{[*]} + \frac{[OH^*]}{[*]} + \frac{[O^*]}{[*]}$$

$$= 1 + K_{CO}(CO) + K_{H_2O}(H_2O) + K_{OH}(H_2O)(H_2)^{-0.5} + K_O(H_2O)(H_2)^{-1}$$

$$\frac{[*]^3}{L^3} = \frac{1}{\left[1 + K_{CO}(CO) + K_{H_2O}(H_2O) + K_{OH}(H_2O)(H_2)^{-0.5} + K_O(H_2O)(H_2)^{-1}\right]^3}$$

Rate Expression:

$$r_{CO,H_2O} = \frac{r_{5d}}{L} = \frac{k_{5d}K_{3d}K_{CO}K_{H_2}^{0.5}K_{H_2O}(CO)(H_2)^{0.5}(H_2O)}{\left[1+K_{CO}(CO)+K_{H_2O}(H_2O)+K_{OH}(H_2O)(H_2)^{-0.5}+K_O(H_2O)(H_2)^{-1}\right]^3} \quad (11)$$

at high CO pressure:

$$r_{CO,H_2O} = \frac{k_{5d}K_{3a}K_{H_2}^{0.5}K_{H_2O}(H_2)^{0.5}(H_2O)}{K_{CO}(CO)} \quad (12)$$

Effective energy barrier at high CO pressure:

$$\Delta E_{eff} = -2Q_{CO} + ½\, Q_{H_2} + Q_{H_2O} + \Delta E_{Rxn,3d} + \Delta E_{Act,5d} \quad (13)$$

$$= \left(2E_{CO(g)} + 2E_* - 2E_{CO^*}\right) + \left(E_{H^*} - E_* - ½\, E_{H_2(g)}\right) + \left(E_{H_2O^*} - E_* - E_{H_2O(g)}\right) + \left(E_{HCO^*} + E_* - E_{H^*} - E_{CO^*}\right) + \left(E_{TS_{5d}^{***}} - E_{HCO^*} - E_{H_2O^*} - E_*\right) \quad (14)$$

$$= E_{TS_{5d}^{***}} + 2E_{CO(g)} - 3E_{CO*} - ½\, E_{H_2(g)} - E_{H_2O(g)} \quad (15)$$

$$= \mathbf{229}\ kJ\ mol^{-1}$$

4) Formyl route with water as a proton shuttling agent

DFT-derived reaction coordinate diagram:

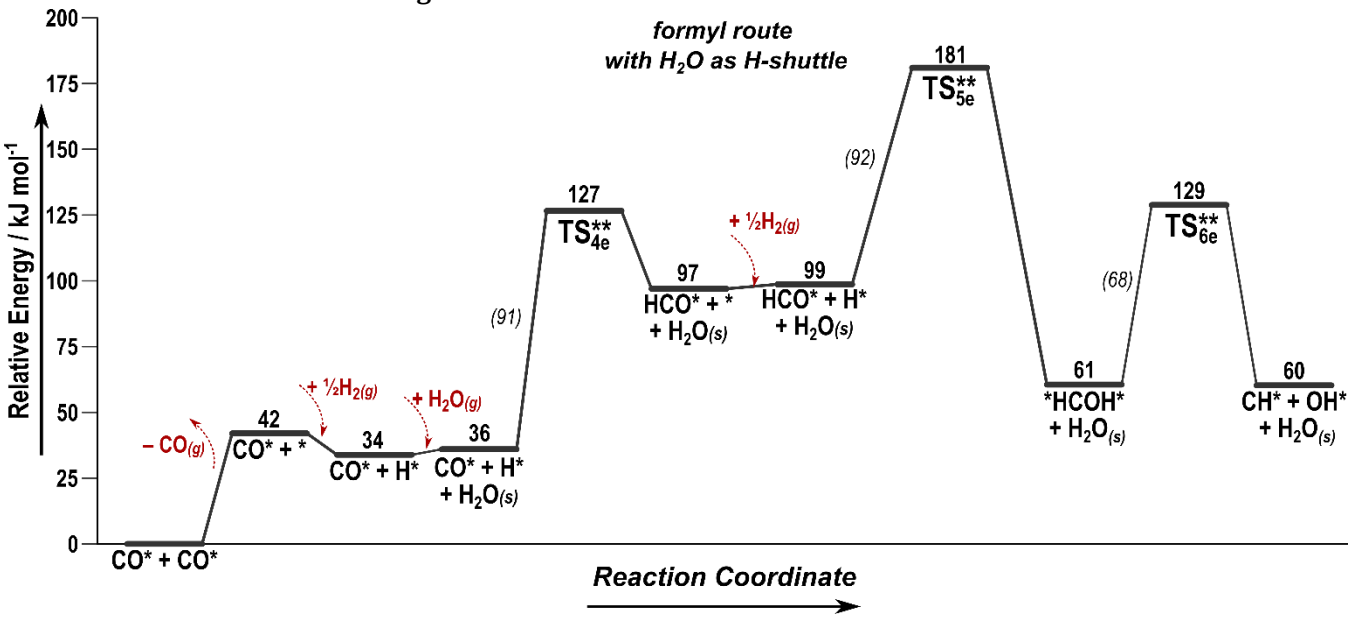

Figure S6. Reaction coordinate diagram for the formyl route with H_2O as a H-shuttle in the formation of *HCOH* and as a solvent during *HCOH* dissociation.

- H_2O must move from the bulk gas phase to a position near the CO*-covered Ru catalyst to act as a solvent or as a H-shuttling agent shown below as step 3. H_2O near the intermediates is designated as H_2O(s) in Figs. S5-6.
- Based on the DFT-derived reaction energies, the formation of HCO* is considered quasi-equilibrated as its reverse activation barrier (30 kJ mol^{-1}) is lower than the forward barrier to form *HCOH* (84 kJ mol^{-1}).
- *HCOH* formation is irreversible as its reverse barrier (120 kJ mol^{-1}) is higher than the forward barrier to form CH* and OH* (68 kJ mol^{-1}).
- For this mechanism, the H_2O-mediated formation of HCOH* via H-shuttling is considered the kinetically-relevant step.

Mechanism

1) $CO(g) + * \rightleftharpoons CO^*$ $\quad [CO^*] = K_{CO}(CO)[*]$

2) $H_2(g) + 2* \rightleftharpoons 2H^*$ $\quad [H^*] = K_{H_2}^{0.5}(H_2)^{0.5}[*]$

3e) $H_2O(g) + CO^* \rightleftharpoons CO^*\cdots H_2O$ $\quad [CO^*\cdots H_2O] = K_s(H_2O)[CO^*]$

4e) $H^* + CO^*\cdots H_2O \rightleftharpoons HCO^*\cdots H_2O + *$ $\quad [HCO^*\cdots H_2O] = K_{4e}K_{CO}K_{H_2}^{0.5}K_s(H_2O)(CO)(H_2)^{0.5}[*]$

5e) $HCO^*\cdots H_2O + H^* \longrightarrow {}^*HCOH^*\cdots H_2O$ $\quad r_{5e} = k_{5e}[HCO^*\cdots H_2O][H^*]L^{-1}$

$= k_{5e}K_{4e}K_{CO}K_{H_2}K_s(CO)(H_2)(H_2O)[*]^2L^{-1}$

6e) $^*HCOH^*\cdots H_2O \longrightarrow CH^* + OH^*\cdots H_2O$

Formation of Site Blocking Intermediates:

$H_2O^* + * \rightleftharpoons OH^* + H^*$ $\quad [OH^*] = K_{OH}(H_2O)(H_2)^{-0.5}[*]$

$OH^* + * \rightleftharpoons O^* + H^*$ $\quad [O^*] = K_O(H_2O)(H_2)^{-1}[*]$

Site Balance:

$$L = [*] + [CO^*] + [H_2O^*] + [OH^*] + [O^*]$$

$$\frac{L}{[*]} = 1 + \frac{[CO^*]}{[*]} + \frac{[H_2O^*]}{[*]} + \frac{[OH^*]}{[*]} + \frac{[O^*]}{[*]}$$

$$= 1 + K_{CO}(CO) + K_{H_2O}(H_2O) + K_{OH}(H_2O)(H_2)^{-0.5} + K_O(H_2O)(H_2)^{-1}$$

$$\frac{[*]^2}{L^2} = \frac{1}{\left[1 + K_{CO}(CO) + K_{H_2O}(H_2O) + K_{OH}(H_2O)(H_2)^{-0.5} + K_O(H_2O)(H_2)^{-1}\right]^2}$$

Rate Expression:

$$r_{CO,H_2O} = \frac{r_{5e}}{L} = \frac{k_{5e}K_{4e}K_{CO}K_{H_2}K_s(CO)(H_2)(H_2O)}{\left[1+K_{CO}(CO)+K_{H_2O}(H_2O)+K_{OH}(H_2O)(H_2)^{-0.5}+K_O(H_2O)(H_2)^{-1}\right]^2}$$

$$r_{CO} = r_{CO,Dry} + r_{CO,H_2O} = \frac{k_{4a}K_{3a}K_{CO}K_{H_2}(CO)(H_2) + k_{5e}K_{4e}K_{CO}K_{H_2}K_s(CO)(H_2)(H_2O)}{\left[1+K_{CO}(CO)+K_{H_2O}(H_2O)+K_{OH}(H_2O)(H_2)^{-0.5}+K_O(H_2O)(H_2)^{-1}\right]^2} \quad (16)$$

at high CO pressure:

$$r_{CO,H_2O} = \frac{k_{5e}K_{4e}K_s(CO)(H_2)(H_2O)}{K_{CO}(CO)} \quad (17)$$

Effective energy barrier at high CO pressure:

$$\Delta E_{eff} = -Q_{CO} + Q_{H_2} + \Delta E_{Rxn,3e} + \Delta E_{Rxn,4e} + \Delta E_{Act,5e} \quad (18)$$

$$= \left(E_{CO(g)} + E_* - E_{CO^*}\right) + \left(2E_{H^*} - 2E_* - E_{H_2(g)}\right) + \left(E_{CO^*\cdots H_2O} - E_{CO*} - E_{H_2O(g)}\right) + \left(E_{HCO^*\cdots H_2O} + E_* - E_{H^*} - E_{CO^*\cdots H_2O}\right) + \left(E_{TS_{5e}^{**}} - E_{HCO^*\cdots H_2O} - E_{H^*}\right) \quad (19)$$

$$= E_{TS_{5e}^{**}} + E_{CO(g)} - 2E_{CO*} - E_{H_2(g)} - E_{H_2O(g)} \quad (20)$$

$$= \mathbf{181}\ kJ\ mol^{-1}$$

5) Hydroxymethylidyne route with water as a solvent and proton shuttling agent

DFT-derived reaction coordinate diagram:

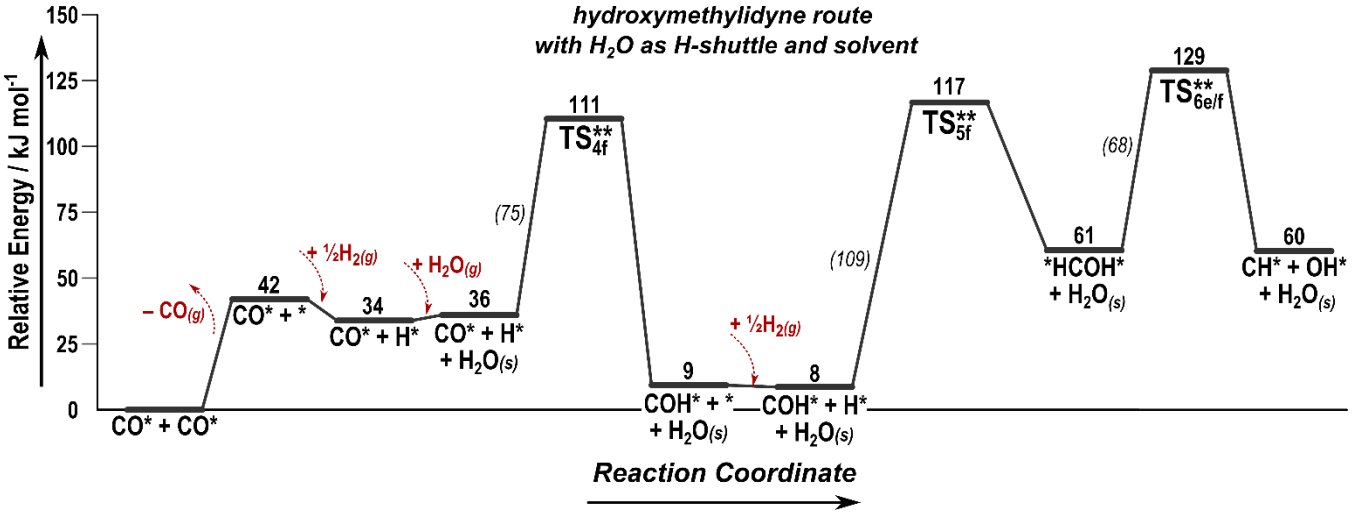

Figure S7. Reaction coordinate diagram for the hydroxymethylidyne route with H_2O as a H-shuttle in the formation of COH* and a solvent during the formation of *HCOH* and *HCOH* dissociation.

- H_2O must move from the bulk gas phase to a position near the CO*-covered Ru catalyst to act as a solvent or a H-shuttle. This step is shown below as step 3. H_2O near the intermediates is designated as $H_2O_{(s)}$ in Figs. S4-5.
- Based on the DFT-derived reaction energies, the formation of HCO* is considered quasi-equilibrated as its reverse activation barrier to form CO* and H* (102 kJ mol^{-1}) is lower than the forward barrier to form *HCOH* (108 kJ mol^{-1}) or dissociate *HCOH* to CH* and OH* (120 kJ mol^{-1}).
- *HCOH* formation is also quasi-equilibrated as its reverse barrier (56 kJ mol^{-1}) is lower than the forward barrier to form CH* and OH* (68 kJ mol^{-1}).
- For this mechanism, the H_2O-solvated dissociation of HCOH* via H-shuttling is considered the kinetically-relevant step.

Mechanism:

1) $CO(g) + * \rightleftharpoons CO^*$ $\quad [CO^*] = K_{CO}(CO)[*]$

2) $H_2(g) + 2* \rightleftharpoons 2H^*$ $\quad [H^*] = K_{H_2}^{0.5}(H_2)^{0.5}[*]$

3f) $H_2O(g) + CO^* \rightleftharpoons CO^*\cdots H_2O$ $\quad [CO^*\cdots H_2O] = K_s(H_2O)[CO^*]$

4f) $H^* + CO^*\cdots H_2O \rightleftharpoons COH^*\cdots H_2O + *$ $\quad [COH^*\cdots H_2O] = K_{4f}K_{CO}K_{H_2}^{0.5}K_s(H_2O)(CO)(H_2)^{0.5}[*]$

5f) $COH^*\cdots H_2O + H^* \rightleftharpoons {}^*HCOH^*\cdots H_2O$ $\quad [{}^*HCOH^*\cdots H_2O] = K_{5f}K_{4f}K_{CO}K_{H_2}K_s(H_2O)(CO)(H_2)[*]^2$

6f) $*HCOH^*\cdots H_2O \longrightarrow CH^* + OH^*\cdots H_2O$ $\quad r_{5b} = k_{6f}[{}^*HCOH^*\cdots H_2O]L^{-1}$

$= k_{6f}K_{5f}K_{4f}K_{CO}K_{H_2}K_s(H_2O)(CO)(H_2)[*]^2$

Formation of Site Blocking Intermediates:

$H_2O^* + * \rightleftharpoons OH^* + H^*$ $\quad [OH^*] = K_{OH}(H_2O)(H_2)^{-0.5}[*]$

$OH^* + * \rightleftharpoons O^* + H^*$ $\quad [O^*] = K_O(H_2O)(H_2)^{-1}[*]$

Site Balance:

$$L = [*] + [CO^*] + [H_2O^*] + [OH^*] + [O^*]$$

$$\frac{L}{[*]} = 1 + \frac{[CO^*]}{[*]} + \frac{[H_2O^*]}{[*]} + \frac{[OH^*]}{[*]} + \frac{[O^*]}{[*]}$$

$$= 1 + K_{CO}(CO) + K_{H_2O}(H_2O) + K_{OH}(H_2O)(H_2)^{-0.5} + K_O(H_2O)(H_2)^{-1}$$

$$\frac{[*]^2}{L^2} = \frac{1}{\left[1 + K_{CO}(CO) + K_{H_2O}(H_2O) + K_{OH}(H_2O)(H_2)^{-0.5} + K_O(H_2O)(H_2)^{-1}\right]^2}$$

Rate Expression:

$$r_{CO,H_2O} = \frac{r_{6f}}{L} = \frac{k_{6f}K_{5f}K_{4f}K_{CO}K_{H_2}K_s(CO)(H_2)(H_2O)}{\left[1+K_{CO}(CO)+K_{H_2O}(H_2O)+K_{OH}(H_2O)(H_2)^{-0.5}+K_O(H_2O)(H_2)^{-1}\right]^2}$$

$$r_{CO} = r_{CO,Dry} + r_{CO,H_2O} = \frac{k_{4a}K_{3a}K_{CO}K_{H_2}(CO)(H_2) + k_{6f}K_{5f}K_{4f}K_{CO}K_{H_2}K_s(CO)(H_2)(H_2O)}{\left[1+K_{CO}(CO)+K_{H_2O}(H_2O)+K_{OH}(H_2O)(H_2)^{-0.5}+K_O(H_2O)(H_2)^{-1}\right]^2} \quad (21)$$

at high CO pressure:

$$r_{CO,H_2O} = \frac{k_{6f}K_{5f}K_{4f}K_{CO}K_{H_2}K_s(CO)(H_2)(H_2O)}{K_{CO}(CO)} \quad (22)$$

Effective energy barrier at high CO pressure:

$$\Delta E_{eff} = -Q_{CO} + Q_{H_2} + \Delta E_{Rxn,3f} + \Delta E_{Rxn,4f} + \Delta E_{Rxn,5f} + \Delta E_{Act,6f} \quad (23)$$

$$= \left(E_{CO(g)} + E_* - E_{CO^*}\right) + \left(2E_{H^*} - 2E_* - E_{H_2(g)}\right) + \left(E_{CO^*\cdots H_2O} - E_{CO*} - E_{H_2O(g)}\right) + \left(E_{COH^*\cdots H_2O} + E_* - E_{H^*} - E_{CO^*\cdots H_2O}\right) + \left(E_{*HCOH^*\cdots H_2O} - E_{H^*} - E_{COH^*\cdots H_2O}\right) + \left(E_{TS_{6f}^{**}} - E_{*HCOH^*\cdots H_2O}\right) \quad (24)$$

$$= E_{TS_{6f}^{**}} + E_{CO(g)} - 2E_{CO*} - E_{H_2(g)} - E_{H_2O(g)} \quad (25)$$

$$= \mathbf{129}\ kJ\ mol^{-1}$$

Extended analysis of Quasi-Equilibrated Assumption for COH* Formation

The formation of COH* is quasi-equilibrated when H_2O-mediated dissociation of COH* (back to CO* and H*) is much faster than net *HCOH* formation rates (from COH* and H*), which equal *HCOH* dissociation rates (CH* and OH*) at steady-state. Quasi-equilibrated COH* formation requires that the ratio of the rate of this step to that of H_2O-mediated COH* dissociation (to CO* and H*):

$$\frac{k_{6f}[\,^{*}HCOH^{*}\cdots H_2O]}{k_{-4f}[*][COH^{*}\cdots H_2O]} = \frac{A_{5f}A_{6f}}{A_{-4f}A_{-5f}}\,exp\left(\frac{E_{act}^{-4f}-\left(E_{act}^{6f}+E_{rxn}^{5f}\right)}{RT}\right)\frac{[H^{*}]}{[*]} \tag{26}$$

be much smaller than unity. For H_2O-mediated routes, the reverse barrier for COH* formation (E_{act}^{-4f} = 102 kJ mol^{-1}) is much smaller than the sum (121 kJ mol^{-1}) of the *HCOH* formation reaction energy (E_{rxn}^{5f} = 53 kJ mol^{-1}) and the *HCOH* dissociation barrier (E_{act}^{6f} = 68 kJ mol^{-1}). This leads to small values of the exponential in Equation 9 (7x10^{-3} at 463 K); (H*)/(*) is much smaller than 1 due to the weak adsorption energy and large loss in entropy upon H* adsorption and the pre-exponential term is of order one because these chemisorbed intermediates have similar entropies.

*IV. Effect of H_2O on the Formation of COH**

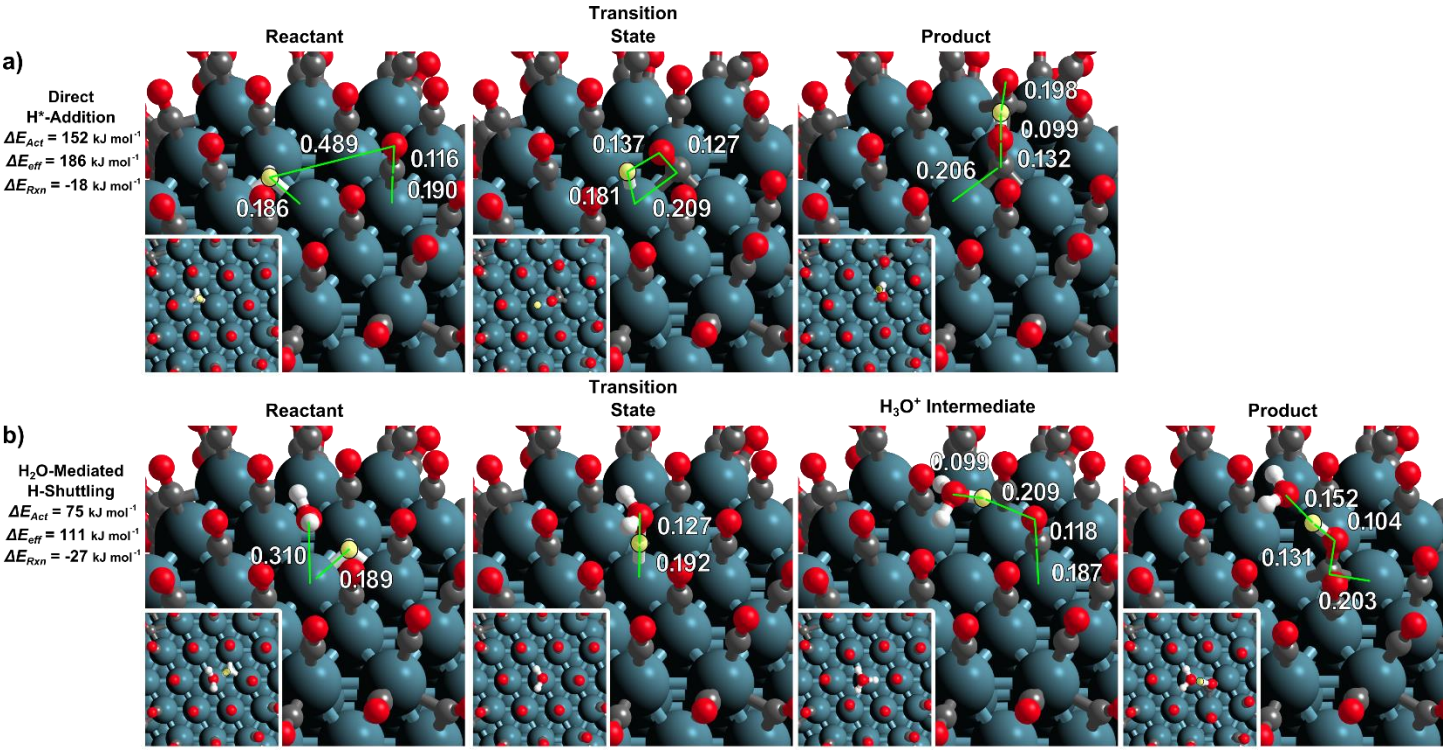

Figure S8. DFT-derived reactant, transition and product states for the formation of COH* a) via H*-addition and b) via H_2O-mediated H-shuttling. Also shown is the DFT-derived structure of the short-lived H_3O^+ intermediate that forms upon the desorption H* and coupled electron transfer to form H^+.

The formation of COH* in the absence of H_2O occurs via O-H bond formation between the O of CO* and H* on the Ru surface. The H* shifts from its stable 3-fold site to a near-atop binding mode in the TS as shown in Fig. S8a. CO* shifts from its stable atop site to a 3-fold site as it bends towards the Ru surface to interact with H*. Once the O-H bond is formed, COH* resides in the 3-fold site, where it is most stable and its O-H bond rotates to interact with a vicinal CO* species. During this sequence, the O-H distance shortens from 0.489 nm in the reactant state to 0.137 nm in the transition state to 0.099 nm in the product state. The intrinsic activation barrier for this reaction is quite large (152 kJ mol^{-1}) despite the negative reaction energy (-18 kJ mol^{-1}).

With H_2O present, the CO* species does not have to lean over to the Ru surface to interact with H* because H_2O can mediate the transfer of H* from the Ru surface to the O of CO* via H-shuttling. Initially, H_2O is not strongly interacting with H*, CO* or the Ru surface (ΔEsolv = +2 kJ mol^{-1}). The H* again shifts from its stable 3-fold site to a near-atop configuration, this time to interact with H_2O resulting in an O-H bond distance of 0.127 nm in the transition state. This forms a short-lived H_3O^+ intermediate which H-bonds with a vicinal CO* (0.209 nm) prior to protonation of that CO* to form COH* which resides in its stable 3-fold site in the product configuration. The intrinsic activation energy is much lower (75 kJ mol^{-1}) via H-shuttling and due to the H-bond between COH* and H_2O, the reaction energy has also decreased (-27 kJ mol^{-1}).

V. Fitting Kinetic Data to a Rate Expression with H_2O-Mediated Routes

H_2O must physisorb near the CO*-covered catalyst particle in order to participate in hydrogenation reactions as described previously. Gas-phase H_2O has an entropy of 204 J mol^{-1} K^{-1} at 463 K[1]. Measurements of physisorbed H_2O give ranges of 60-80 J mol^{-1} K^{-1},[2] indicating a ΔS_{ads} of 124-144 J mol^{-1} K^{-1}. If the H_2O has condensed inside the microporous environment of the support, we can estimate the entropy of the H_2O in liquid phase to be 70 J mol^{-1} K^{-1},[1] which is very similar to the estimates of the entropy of physisorbed H_2O, resulting in a ΔS_{ads} of 134 J mol^{-1} K^{-1}.

If we treat the DFT-derived energies as enthalpies, we can estimate the difference between the free energy barrier for the anhydrous and H_2O-mediated paths to be:

$$\Delta G_{Anhyd.} - \Delta G_{H_2O-med.} = \left(\Delta H_{Anhyd.} - \Delta H_{H_2O-med.}\right) - T\left(\Delta S_{Anhyd.} - \Delta S_{H_2O-med.}\right) \quad (27)$$

and we can approximate that the largest contributor to the difference in entropies between the anhydrous and H_2O-mediated routes to be the adsorption of H_2O:

$$\Delta G_{Anhyd.} - \Delta G_{H_2O-med.} = \left(\Delta H_{Anhyd.} - \Delta H_{H_2O-med.}\right) - T\left(\Delta S_{H_2O,ads}\right) \quad (28)$$

which gives differences in the free energy barrier between +7 and -3 kJ mol^{-1} at 463 K:

$$\Delta G_{Anhyd.} - \Delta G_{H_2O-med.} = (193 - 129)\text{kJ mol}^{-1} - 463\text{ K}(134 \pm 10\text{ J mol}^{-1}\text{K}^{-1}) \quad (29)$$

$$\Delta G_{Anhyd.} - \Delta G_{H_2O-med.} = 2 \pm 5\text{ kJ mol}^{-1} \quad (30)$$

[1] Chase, M.W., Jr., NIST-JANAF Themochemical Tables, Fourth Edition, J. Phys. Chem. Ref. Data, Monograph 9, 1998, 1-1951.
[2] M. Nagao, *J. Phys. Chem.* **1971**, *75*, 3822.

VI. Fitting Kinetic Data to a Rate Expression with H_2O-Mediated Routes

$$r_{CO} = \frac{\alpha(CO)(H_2)+\beta(CO)(H_2)(H_2O)}{\left[1+K_{CO}(CO)+K_{H_2O}(H_2O)+K_{OH}(H_2O)(H_2)^{-0.5}+K_O(H_2O)(H_2)^{-1}\right]^2} \quad (31)$$

$$K_{H_2O} = \frac{[H_2O^*]}{[*](H_2O)} \qquad K_{OH} = \frac{[OH^*](H_2)^{0.5}}{[*](H_2O)} \qquad K_O = \frac{[O^*](H_2)}{[*](H_2O)}$$

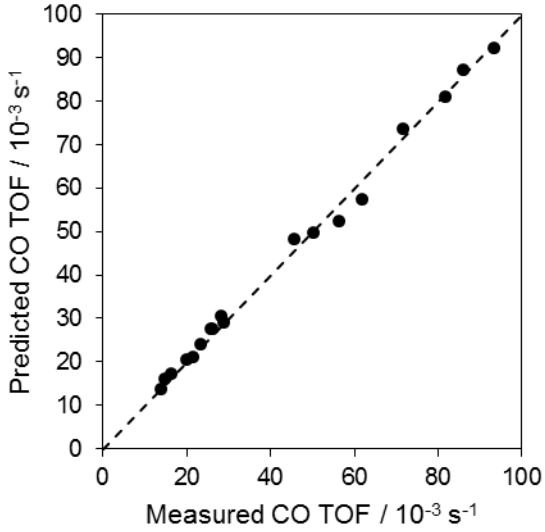

Figure S9. Parity plot comparing the predicted CO consumption turnover rate from Equation 10 with fit parameters shown in Table 1 and the measured CO consumption turnover rate.

Table S1. Best-fit values for the lumped rate constants α and β and the CO and H_2O adsorption constants (K_{CO} and K_{H2O}) for FTS on SiO_2-supported 7 nm Ru clusters at 463 K.

	$\boldsymbol{\alpha}$ *mol s^{-1} mol Ru^{-1} MPa^{-2}*	$\boldsymbol{\beta}$ *mol s^{-1} mol Ru^{-1} MPa^{-3}*	$\boldsymbol{K_{CO}}$ *MPa^{-1}*	$\boldsymbol{K_{H_2O}}$ *MPa^{-1}*	$\boldsymbol{K_{OH}}$ *$MPa^{-0.5}$*	$\boldsymbol{K_O}$
Ref 10a also on 7 nm Ru	0.58 ± 0.08	--	5.6 ± 0.6	--	--	--
This Work	0.66 ± 0.11	4.72 ± 1.1	6.2 ± 0.7	0-3.1	0-3.9	0-5.1

$$\alpha = k_{4a}K_{3a}K_{CO}K_{H_2} \qquad \beta = k_{6f}K_{5f}K_{4f}K_{3f}K_{CO}K_{H_2}$$

Sensitivity Analyses on K_{H_2O}, K_{OH}, and K_O

Table S2. Sensitivity Analyses for K_{H_2O}, K_{OH}, and K_O. Each bold parameter was specified, allowing all other parameters to be fit to determine how the quality of the fit, as calculated by the sum of square residuals (SSR) varies with the values of K_{H_2O}, K_{OH}, and K_O. A parity plot showing the shaded rows is included in Fig. S11

K_{H_2O} *MPa^{-1}*	K_{OH} *MPa$^{-0.5}$*	K_O	α *mol s^{-1} mol Ru^{-1} MPa^{-2}*	β *mol s^{1} mol Ru^{-1} MPa^{-3}*	K_{CO} *MPa^{-1}*	SSR
0.0	0.0	5.1	0.65	4.14	6.15	835
0.5	0.0	4.3	0.66	4.24	6.17	839
1.0	0.0	3.5	0.66	4.35	6.18	844
1.5	0.0	2.6	0.66	4.45	6.20	849
2.0	0.0	1.8	0.66	4.56	6.22	854
2.5	0.0	1.0	0.66	4.66	6.24	859
3.0	0.0	0.2	0.66	4.77	6.26	865
3.1	**0.0**	**0.0**	0.66	4.72	6.23	866
3.5	0.0	0.0	0.53	4.46	5.42	890
0.0	**0.0**	5.1	0.65	4.14	6.15	835
0.0	**0.5**	4.5	0.65	4.18	6.16	836
0.0	**1.0**	3.8	0.66	4.21	6.16	838
0.0	**1.5**	3.2	0.66	4.25	6.17	840
0.0	**2.0**	2.5	0.66	4.29	6.17	842
0.0	**2.5**	1.9	0.66	4.32	6.18	844
0.0	**3.0**	1.3	0.66	4.36	6.19	846
0.0	**3.5**	0.6	0.66	4.40	6.19	848
0.0	3.9	**0.0**	0.66	4.40	6.19	850
0.0	**4.5**	0.0	0.69	4.99	6.46	873
0.0	3.6	**0.5**	0.66	4.37	6.18	849
0.0	3.2	**1.0**	0.66	4.35	6.18	847
0.0	2.8	**1.5**	0.66	4.32	6.17	845
0.0	2.4	**2.0**	0.65	4.29	6.17	844
0.0	2.0	**2.5**	0.65	4.26	6.16	842
0.0	1.6	**3.0**	0.65	4.23	6.16	841
0.0	1.2	**3.5**	0.65	4.21	6.15	839
0.0	0.8	**4.0**	0.65	4.18	6.15	838
0.0	0.5	**4.5**	0.65	4.15	6.14	836
0.0	0.1	**5.0**	0.65	4.12	6.14	835
0.0	0.0	**5.1**	0.65	4.14	6.15	835
0.0	0.0	**5.5**	0.67	4.42	6.29	841
0.0	0.0	**6.0**	0.70	4.80	6.48	868

As shown in Table S2, the sum of squared residuals (SSR) is between 835 and 866 as K_{H_2O} is varied between 0 and 3.1 and K_O changes from 5.1 to 0 over this range, K_{OH} is constant at 0 and α is nearly constant while β and K_{CO} both increase with increasing K_{H_2O}. Above a K_{H_2O} value of 3.1, the SSR sharply increases, as shown in Fig. S10. Similar trends can be observed for K_{OH} and K_O.

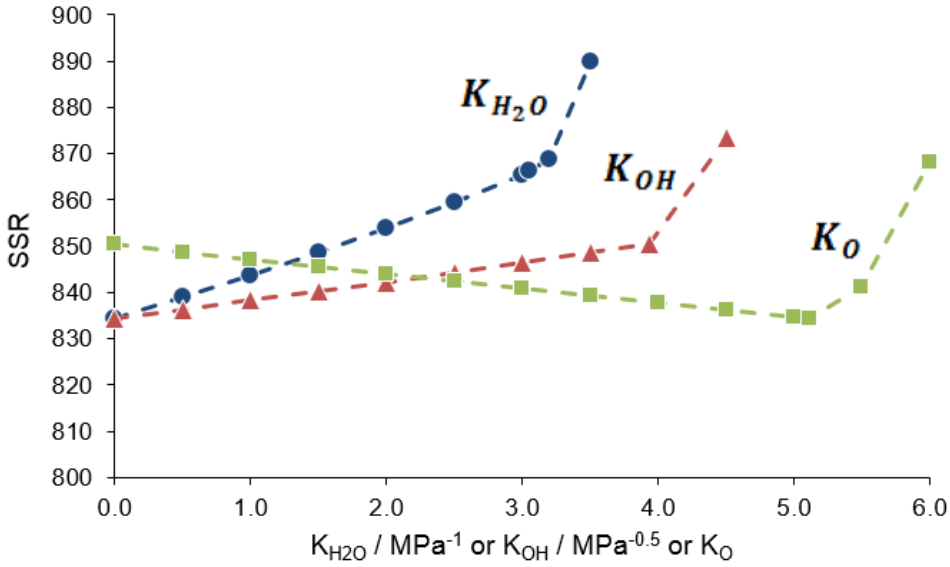

Figure S10. Effect of for K_{H_2O}, K_{OH}, and K_O on the SSR for the model shown in Eq. S26.

The minimum SSR observed over this range is 835 and corresponds to values of 0, 0 and 5.1 for K_{H_2O}, K_{OH}, and K_O, respectively. The maximum SSR observed over the range reported in Table S1 is 869, corresponding to values of 3.1, 0 and 0 for K_{H_2O}, K_{OH}, and K_O, respectively. In order to determine how distinct the fits are between these two sets of parameters, a parity plot was generated (Fig. S11) which shows that these two sets of parameters produce nearly identical sets of predicted data, indicating that despite the decrease change in SSR, the quality of the fit is essentially unaffected over the range of K_{H_2O}, K_{OH}, and K_O shown in Table S1.

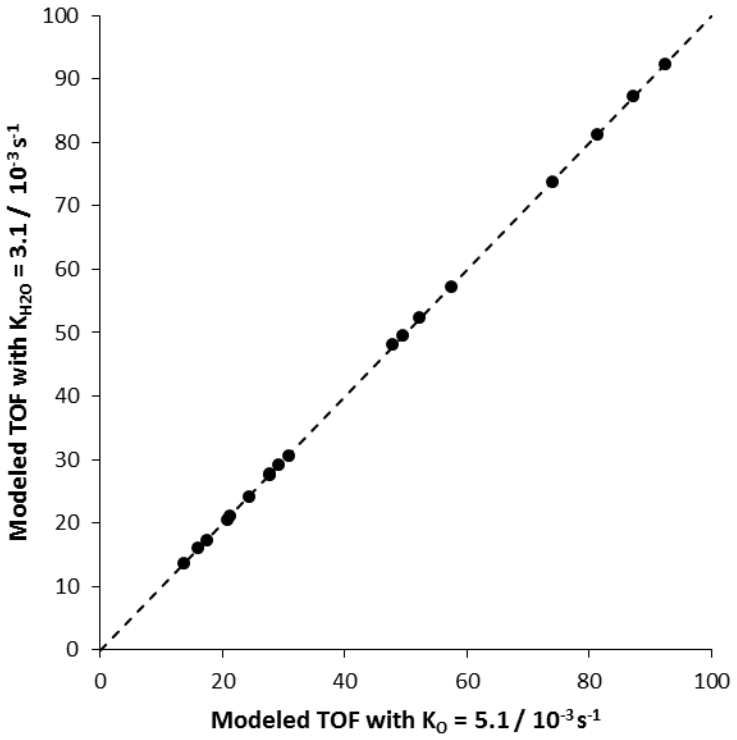

Figure S11. A comparison of Eq. S26 with two sets of parameters (Rows 1 and 8 in Table S2), one without contributions from OH* or O* (K_{H_2O} = 3.1 MPa^{-1}, K_{OH}, and K_O = 0) and one without contributions from H_2O* or OH* (K_O = 5.1, K_{H_2O}, and K_{OH} = 0)

VII. Stability of H_2O, OH* and O* adsorbates*

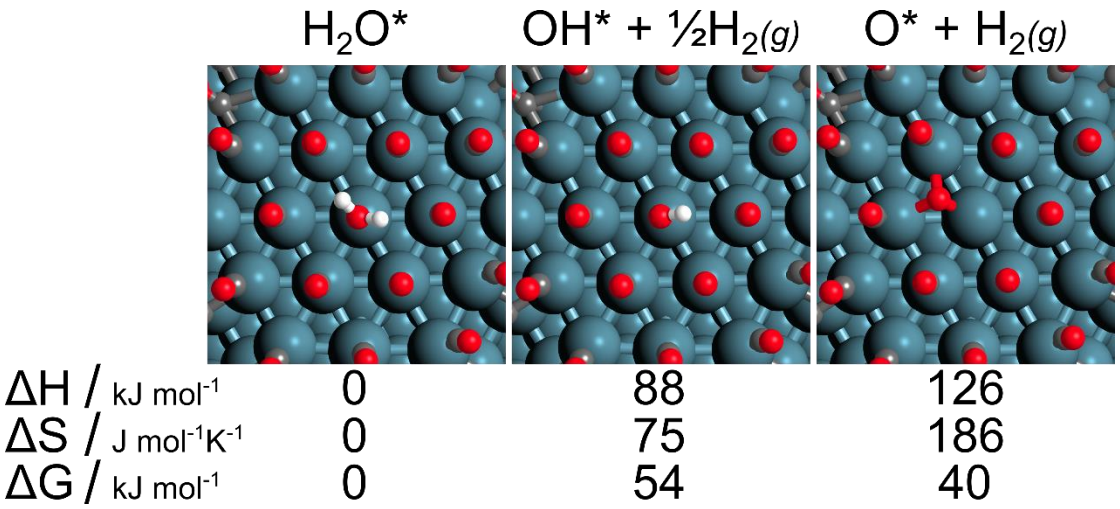

Figure S12. DFT-derived structures and relative stabilities of each of the H_2O-derived species (H_2O*, OH*, and O*) in the denominator of the H_2O-included Langmuir-Hinshelwood Eqs. presented below.

$$r_{CO} = \frac{\alpha(CO)(H_2)+\beta(CO)(H_2)(H_2O)}{\left[1+K_{CO}(CO)+K_{H_2O}(H_2O)+K_{OH}(H_2O)(H_2)^{-0.5}+K_O(H_2O)(H_2)^{-1}\right]^2} \quad (32)$$

DFT-derived energies predict that H_2O* is the most stable H_2O-derived intermediate, followed by O* and then OH*. For these calculations, the entropy of H_2O*, OH*, and O* is assumed to be constant, as such the ΔS between H_2O* and OH* and O* accounts only for the entropy of gas-phase H_2 obtained from ideal gas partition functions. The ΔG values can be used to estimate ratios of adsorption constants:

$$\frac{K_{OH}}{K_{H_2O}} = e^{\left(\frac{G_{OH^*}+G_{½H_2(g)}-G_{H_2O^*}}{RT}\right)} = 9\text{x}10^{-7}\ MPa^{0.5}$$

$$\frac{K_O}{K_{H_2O}} = e^{\left(\frac{G_{O^*}+G_{H_2(g)}-G_{H_2O^*}}{RT}\right)} = 3\text{x}10^{-5} MPa$$

As the ratios of K_{OH} and K_O to K_{H_2O} are $\ll 1$ and H_2 pressures are typically > 1 MPa, it is unlikely that OH* or O* exists at significant coverages relative to H_2O*:

$$\frac{[OH^*]}{[H_2O^*]} = \frac{K_{OH}(H_2O)(H_2)^{-0.5}}{K_{H_2O}(H_2O)} = \frac{K_{OH}}{K_{H_2O}(H_2)^{0.5}}$$

$$\frac{[O^*]}{[H_2O^*]} = \frac{K_O(H_2O)(H_2)^{-1}}{K_{H_2O}(H_2O)} = \frac{K_O}{K_{H_2O}(H_2)}$$

VIII. Influence of H_2O on Chain Growth Probabilities

Chain growth can occur either via coupling of activated C_1 intermediates (CH_x*) with growing alkyl chains on the catalyst surface (C_nH_{2n+1}*), Eq. 33, or via CO*-insertion into growing alkyl chains, Eq. 34. If CO*-insertion is reversible, then the H-addition to the acyl intermediate ($C_nH_{2n+1}CO$*) is the propagation-limiting step which is followed by C-O activation to form $C_nH_{2n+1}C$* and OH* (Eq. 35b).

$C_nH_{2n+1}* + CH_x* \longrightarrow C_{n+1}H_{2n+1+x}* + *$ $\quad r_{P,33} = k_{33}[C_nH^*_{2n+1}][CH^*_x]$ (33)

$C_nH_{2n+1}* + CO* \longrightarrow C_nH_{2n+1}CO* + *$ $\quad r_{P,34} = k_{34}[C_nH^*_{2n+1}][CO^*]$ (34)

$C_nH_{2n+1}* + CO* \rightleftharpoons C_nH_{2n+1}CO* + *$ $\quad [C_nH_{2n+1}CO^*] = K_{35a}[C_nH^*_{2n+1}][CO^*][*]^{-1}$ (35a)

$C_nH_{2n+1}CO* + H* \longrightarrow C_nH_{2n+1}C* + OH*$ $\quad r_{P,35} = k_{35b}K_{35a}[C_nH^*_{2n+1}][CO^*][*]^{-1}[H^*]$ (35b)

Thus, there are three possible propagation-limiting reactions, leading to three different propagation rates ($r_{P,26,27,28}$), while the reaction energies and barriers for these reactions will be investigated in a future work, for this manuscript we will consider the effect of H_2O on all three possibilities.

Termination occurs either via β-H elimination of the alkyl chain to form a terminal alkene (for n>1), Eq. 36, or via H-addition to the alkyl chain to form n-alkanes (for all n), Eq. 37.

$C_nH_{2n+1}* + * \rightarrow C_nH_{2n}* + H*$ $\quad r_{T,36} = k_{36}[C_nH^*_{2n+1}][*]$ (36)

$C_nH_{2n+1}* + H* \rightarrow C_nH_{2n+2}* + *$ $\quad r_{T,37} = k_{37}[C_nH^*_{2n+1}][H^*]$ (37)

Thus, for all products other than methane (n>1), the ratio of propagation to termination can be defined using either Eq. 33, 34 or 35 for rates of propagation.

Case 1: when propagation occurs via alkyl coupling with an activated C_1 species (Eq. 33), the chain-growth probability is:

$$\eta_{33} = \frac{r_{P,33}}{r_{T,36}+r_{T,37}} = \frac{k_{33}[C_nH^*_{2n+1}][CH^*_x]}{k_{36}[C_nH^*_{2n+1}][*]+k_{37}[C_nH^*_{2n+1}][H^*]} = \frac{k_{33}[CH^*_x]}{k_{36}[*]+k_{37}[H^*]} \quad (38)$$

CH_x* species are produced via CO*-activation that is promoted by H_2O, and as none of Rxns 33, 36 or 37 involve polar reactant, transition or product states, it is unlikely that H_2O could act as a solvent or H-shuttle to alter the rate constant or provide H_2O-mediated paths. Thus, H_2O is increasing the rate of production of CH_x* without concomitant increases in its consumption, resulting in an increase in [CH_x*], increasing the chain-growth probability, η_{26}.

Case 2: when propagation is limited by CO* insertion into alkyl chains (Eq. 34), the chain-growth probability is:

$$\eta_{34} = \frac{r_{P,34}}{r_{T,36}+r_{T,37}} = \frac{k_{34}[C_nH^*_{2n+1}][CO^*]}{k_{36}[C_nH^*_{2n+1}][*]+k_{37}[C_nH^*_{2n+1}][H^*]} = \frac{k_{34}[CO^*]}{k_{36}[*]+k_{37}[H^*]} = \frac{k_{34}K_{CO}(CO)}{k_{36}+k_{37}K_{H_2}^{0.5}(H_2)^{0.5}} \quad (39)$$

As shown, in this case, the chain-growth probability depends only on the relative coverages of CO*, H* and vacant sites (*), which are unaffected by H_2O pressure. As mentioned, the termination reactions (Rxns 36 or 37) do not involve polar reactant, transition or product states, so it is unlikely that H_2O could act as a solvent or H-shuttle to alter the rate constant or provide H_2O-mediated paths. Thus, the only way which H_2O could alter the chain-growth probability is by acting as a solvent during the CO*-insertion reaction, Eqn. 34, reducing the effective activation barrier and thus promoting propagation over termination. Whether H_2O will influence this reaction will be explored in a later work.

Case 3: when propagation occurs via a quasi-equilibrated CO*-insertion (Eq. 35a) followed by a propagation-limiting H*-addition step to form *$C_nH_{2n+1}COH$* (Eq. 35b) followed by dissociation to form $C_nH_{2n+1}C$* + OH*:

$$\eta_{35} = \frac{r_{P,35}}{r_{T,36}+r_{T,37}} = \frac{k_{35b}K_{35a}[C_nH^*_{2n+1}][CO^*][*]^{-1}[H^*]}{k_{36}[C_nH^*_{2n+1}][*]+k_{37}[C_nH^*_{2n+1}][H^*]} = \frac{k_{35b}K_{35a}[CO^*][*]^{-1}[H^*]}{k_{36}[*]+k_{37}[H^*]} = \frac{k_{35b}K_{35a}K_{CO}(CO)K_{H_2}^{0.5}(H_2)^{0.5}}{k_{36}+k_{37}K_{H_2}^{0.5}(H_2)^{0.5}} \quad (40)$$

Here, the propagation-limiting step is analogous to H*-addition to *HCO* to form *HCOH* followed by *HCOH* dissociation to form CH* and OH*. This is simply Eq. 35b with n=0. As shown earlier, H_2O can mediate the H*-addition to HCO* via a H-shuttling pathway and we expect that H_2O can mediate H*-addition to $C_nH_{2n+1}CO$* via an analogous pathway, resulting in an additive term to Eq. 40 to account for H_2O-mediated propagation.

$$\eta_{35} = \frac{r_{P,35}}{r_{T,36}+r_{T,37}} = \frac{k_{35b}K_{35a}K_{CO}(CO)K_{H_2}^{0.5}(H_2)^{0.5}+k_{35b,w/H_2O}K_{35a}K_{CO}(CO)K_{H_2}^{0.5}(H_2)^{0.5}(H_2O)}{k_{36}+k_{37}K_{H_2}^{0.5}(H_2)^{0.5}} \quad (41)$$